

Low-frequency regime transitions and predictability of regimes in a barotropic model

B. T. Nadiga and T.J. O’Kane

May 20, 2016

Contents

0.1	Abstract	1
0.2	Introduction	2
0.3	The barotropic vorticity model and its numerical discretization	7
0.4	Low-frequency variability and regime transitions	8
0.5	Ensemble Perturbations	10
0.6	Predictability in Zonal and Dipolar Regimes	11
0.7	Ensemble behavior in terms of error and spread	14
0.8	Flow stability and sensitivity of BVs to rescaling amplitude and period	19
0.8.1	Dependence of error and spread on perturbation rescal- ing period	22
0.8.2	Error and spread of random rescaling BV perturbations	24
0.9	The role of small scales	24
0.10	Discussion and conclusion	25
0.11	acknowledgments	31

0.1 Abstract

The predictability of flow is examined in a barotropic vorticity model that admits low frequency regime transitions between zonal and dipolar states. Low-frequency regime transitions in the model were first studied by Bouchet and Simonnet (2009) and are reminiscent of regime change phenomena in the weather and climate systems wherein extreme and abrupt qualitative changes occur, seemingly randomly, after long periods of apparent stability. Mechanisms underlying regime transitions in the model are not well understood yet. From the point of view of atmospheric and oceanic dynamics, a novel aspect of the model is the lack of any source of background gradient of potential-vorticity such as topography or planetary gradient of rotation rate (e.g., as considered by Charney and DeVore, 1979).

We consider perturbations that are embedded onto the system’s chaotic attractor under the full nonlinear dynamics as bred vectors—nonlinear generalizations of the leading (backward) Lyapunov vector. We find that ensemble predictions that use bred vector perturbations are more robust in terms of error-spread relationship than those that use Lyapunov vector perturbations. In particular, when bred vector perturbations are used in conjunction with a simple data assimilation scheme (nudging to truth) that estimates the current state of the system, we find that at least some of the evolved perturbations align to identify low-dimensional subspaces associated with regions of large forecast error in the control (unperturbed, data-assimilating) run; this happens less often in ensemble predictions that use Lyapunov vector perturbations. Nevertheless, in the inertial regime we consider, we find that (a) the system is more predictable when it is in the zonal regime, and that (b) the horizon of predictability is far too short compared to characteristic time scales associated with processes that lead to regime transitions, thus precluding the possibility of predicting such transitions.

0.2 Introduction

The phenomenon of blocking—large-scale patterns in the atmospheric pressure field that are nearly stationary—in the extra-tropical winter atmosphere (e.g., Charney and DeVore, 1979) is one of the best studied cases of regime transitions that occur in the weather and climate systems. Other such phenomena include bimodality of the Kuroshio extension system (Qiu and Miao, 2000) wherein beta and topographic effects lead to two preferred meander patterns for the Kuroshio current south of Japan and Dansgaard-Oeschger (D-O) events (e.g., Dansgaard et al., 1989)—25 events during the last glacial period that involved rapid warming followed by gradual cooling with a recurrence time of about 1500 years.

Clearly regime transitions can occur due to a variety of reasons. For example, for atmospheric blocks, quasi-stationary Rossby wave trains and synoptic-scale transient eddies are recognized as playing a role (e.g., see Nakamura et al., 1997, and references therein), whereas beta and topographic effects are seen to be important in the bi-modality of the Kuroshio current. (Causes of D-O events are less clear.) In the context of atmospheric blocking, Charney and DeVore (1979) proposed a multiple equilibria hypothesis whereby the atmosphere possesses multiple stable steady states corresponding to observed multiple weather regimes. The setting in this study and numerous others that followed consisted of a barotropic model

with topography. It is, however, interesting to note that while topography (or other sources of background gradients in potential vorticity) are not necessary for the transient eddy mechanism mentioned above, most studies have indeed included such sources of background gradients in potential vorticity. We are not aware of studies of low-frequency regime transitions that do not include such sources. It is in this context that the recent work of Bouchet and Simonnet (2009) (referred to as BS09 for brevity) fills a gap: The model they consider has no background gradient of potential vorticity (as due to a gradient of planetary rotation rate or due to topography,) and therefore no (planetary or topographic) Rossby waves. Nevertheless, when the model is subjected to weak stochastic forcing representative of inherently unpredictable, or unresolved physics, irregular low-frequency zonal-dipolar regime transitions arise.

The advantage of this model is that while on the one hand, its behavior is reminiscent of regime change phenomena in the ocean and climate systems wherein extreme and abrupt qualitative changes occur, seemingly randomly, after very long periods of apparent stability, on the other, it is simple enough that it is likely to yield to better understanding of the dynamics underlying such phenomena. We note that the dynamics of transitions in the model can be described in different manners. For example, BS09 explain observed regime transitions in the model in terms of phase transitions between dipolar structures and unidirectional flows. (For details, the reader is referred to BS09.) On the other hand, in an unforced setting, Loxley and Nadiga (2013) (hereafter referred to as LN13) consider a simple theory for predicting quasi-steady states that combines a maximum entropy principal with a nonlinear parameterization of the vorticity-stream-function dependency. We briefly digress to discuss this explanation of regime transitions since it instigates the possibility that regime transitions can be predicted.

The theory of LN13 predicts that when the aspect ratio is varied, unidirectional flows are bistable, exhibit hysteresis, and undergo large abrupt changes in flow topology whereas dipolar structures undergo continuous changes in flow topology. These results are summarized in Figs. 1 and 2 wherein values of $\bar{\psi}_1^2/2$ for long-lived states at different values of aspect ratio are shown for a large number of decaying turbulence simulations on a domain $(0, 2\pi\delta) \times (0, 2\pi/\delta)$. Here, $\bar{\psi}_1$ is the amplitude of the eigenmode with the largest spatial scale in the east-west or x direction. In Fig. 1, the vorticity-stream-function dependency is tanh-like and leads to unidirectional flows. In this figure, a value of $\bar{\psi}_1^2/2 \approx 0$ corresponds to unidirectional flow along the x -axis (Fig. 1, left inset), while $\bar{\psi}_1^2/2 \approx 1$ corresponds to unidirectional flow along the y -axis (Fig. 1, right inset). Different symbols cor-

respond to different sets of experiments where the initial conditions and/or small scale dissipation were varied. Two branches of stable states are clearly seen in that figure: the lower branch corresponds to unidirectional flow along the x -axis; and the upper branch, to unidirectional flow along the y -axis. These states coexist in a bistable region for some range of δ -values where δ is the square-root of the aspect ratio (ratio of the size of the domain in the east-west or x direction to that in the north-south or y direction).

In Fig. 2, the vorticity-stream-function dependency is sinh-like and this leads to dipolar states. In this figure, a value of $\bar{\psi}_1^2/2 \approx 0.5$ corresponds to a vortex pair with flow components along both the x - and y -axes (Fig. 2, Left Inset), while deviations towards smaller or larger values of $\bar{\psi}_1^2/2$ indicate the tendency towards a more unidirectional flow (e.g., Fig. 2, Right Inset). In contrast to Fig. 1, a single branch of stable states is seen in Fig. 2 as δ is varied. In the middle of this branch is a single vortex pair in a square domain (Fig. 2, left inset). As δ is increased, this state is continuously “squeezed” along the y -axis—eventually yielding a large component of unidirectional flow along the y -axis (Fig. 2, right inset). Similarly, decreasing δ eventually leads to a large component of unidirectional flow along the x -axis. To a good approximation a continuous change in flow topology from a vortex pair to a unidirectional flow takes place as δ is changed: there is no sudden large change in flow topology as in Fig. 1.

To have large random changes between a unidirectional flow and a dipolar structure requires both states to be quasi-steady states. Except that they are quasi-steady states not at the same time, but at nearby points in time. Thus, the mechanism hypothesized by LN13 to explain the random changes between a unidirectional flow and a dipolar structure is as follows: Only one of the flow structures (unidirectional flow or dipole) is a quasi-steady state over a short timescale, and decaying turbulence causes relaxation towards that state. Over a longer timescale, however, it is the cumulative effect of the weak stochastic forcing that leads (randomly) to the other state being the (now sole) preferred quasi-steady state and to which it relaxes on the shorter timescale. Indeed this mechanism leads to the prediction that a regime transition is preceded by a change in the kurtosis of the vorticity distribution. The question then arises as to whether such behavior can be used to predict regime transitions in the model. But, before considering that question, we characterize differences in predictability of the zonal and dipolar regimes and study the role of small scales in prediction and their role in initiating regime transitions.

We now return from the digression. That abrupt changes that can occur in the real weather and climate systems may be the result of small,

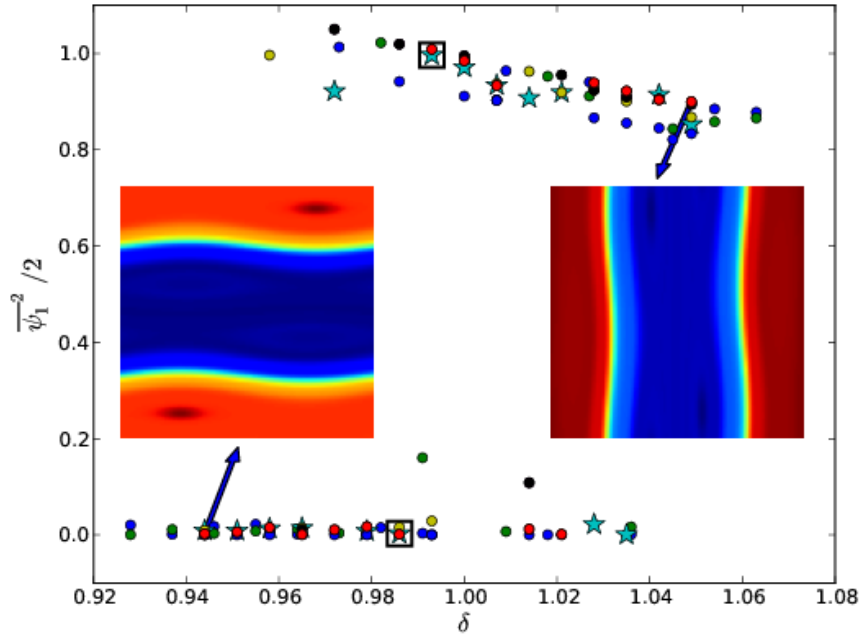


Figure 1: The behavior of long-lived unidirectional flow states for different values of δ where δ is the square-root of the aspect ratio. A value of $\bar{\psi}_1^2 / 2 \approx 0$ corresponds to unidirectional flow along the x -axis (left inset), while $\bar{\psi}_1^2 / 2 \approx 1$ corresponds to unidirectional flow along the y -axis (right inset). Note hysteresis and abrupt changes with respect to aspect ratio. Different symbols correspond to different sets of experiments where the initial conditions and/or small scale dissipation were varied. Adapted from LN13.

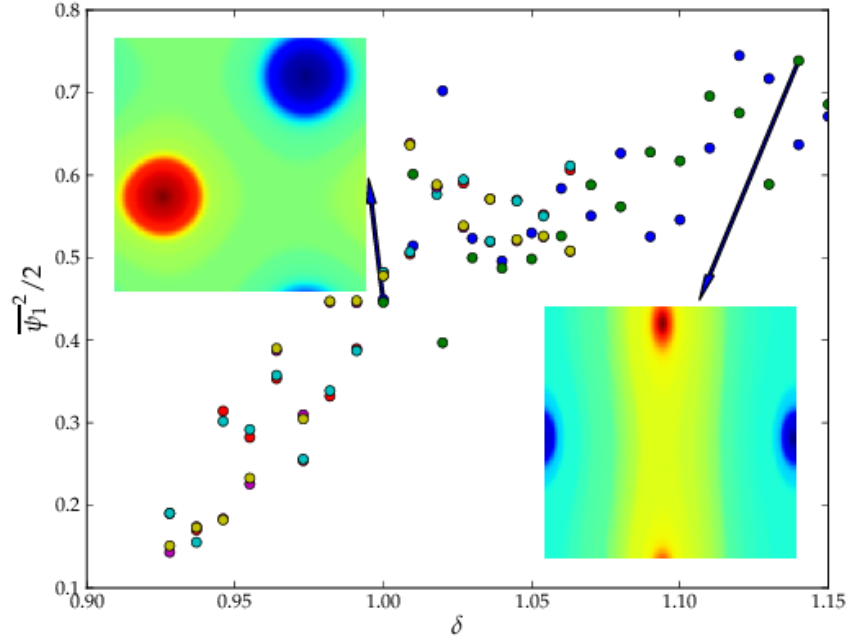


Figure 2: The behavior of long-lived dipolar flow states for different values of δ where δ is the square-root of the aspect ratio. A value of $\bar{\psi}_1^2/2$ of 0.5 corresponds to a vortex pair with flow components along both the x- and y-axes (left inset), while deviations towards smaller or larger values indicate the tendency towards a more unidirectional flow (right inset). A more continuous change in flow is seen with respect to changes in aspect ratio. Adapted from LN13.

inherently unpredictable, or unresolved processes (e.g. see Frederiksen and O’Kane (2008)) is accounted for by the weak and stochastic nature of the forcing in this model. In the parameter regime we consider, the effect of the stochastic forcing when the model is in one of the zonal or dipolar regimes itself is minimal. However, the model displays no regime transitions in the absence of stochastic forcing, and this is consistent with the mechanism of LN13 described previously. Consequently, the occasional, large (nonlinear) response of the system (regime shifts) to weak stochastic forcing, and which response is unrelated to matching a natural frequency of the system suggests a form of stochastic resonance (Benzi et al. (1982), or e.g., see Williams et al. (2003))—a constructive concurrence of nonlinearity and noise—in setting up the regime transitions. In this model, the underlying quasi-stable states essential to such a mechanism are more dynamical than say the quasi-steady states of the Kuroshio system. That is, whereas in the Kuroshio context, the quasi-steady states are determined by specified topography, in the present model the quasi-steady states are those anticipated by statistical mechanical theories for the large scales of the system (e.g., the Robert-Sommeria-Miller theory Chavanis and Sommeria (1996)). Further, the difference in the nature of the quasi-steady states is reflected (and captured) by differences in the vorticity-streamfunction relationship and differences in the kurtosis of the vorticity distribution itself.

0.3 The barotropic vorticity model and its numerical discretization

We consider the stochastically forced barotropic vorticity equation on the f -plane:

$$\frac{D\omega}{Dt} = \frac{\partial\omega}{\partial t} + \mathbf{u} \cdot \nabla\omega = F + D \quad (1)$$

on a horizontal rectangular domain $2\pi\delta \times 2\pi/\delta$ with an aspect ratio δ^2 . Here, ω is the vertical vorticity given in terms of streamfunction ψ by $\omega = \nabla^2\psi$, \mathbf{u} is velocity given by $\mathbf{u} = \mathbf{e}_z \times \nabla\psi$, F is forcing and D is dissipation. Dissipation consists of linear damping: $-\alpha\omega$, where α is a frictional constant; and a small-scale dissipation term that is a sink of the net-forward cascading enstrophy. The small scale dissipation is implemented as a high pass filter of the vorticity field with a characteristic wavenumber k_d ($\approx 0.61k_{max}$, where k_{max} is the maximum wavenumber of the simulation). Forcing F is scaled as $F = \sqrt{2\alpha}\tilde{F}$, where \tilde{F} is an isotropic stochastic forcing in a small band of wavenumbers $2 \leq k_f < 3$ drawn from independent

unit variance Gaussian distributions and which is temporally uncorrelated: $\langle \tilde{F}_{\mathbf{k}}(t)\tilde{F}_{\mathbf{k}'}(t') \rangle = \delta_{\mathbf{k}\mathbf{k}'}(t-t')$. (A wide variety of other spectral forcings considered produced similar dipolar-zonal transitions.) If energy predominantly resides in the large scales, then energy is mainly dissipated by linear damping. In that case, the chosen scaling of forcing and linear damping terms renders the long-time average of energy in a statistical stationary state unity. Under these circumstances, the nondimensional time is measured in terms of eddy turnover times where an eddy turnover time is L_{ref}/U_{ref} and given a dimensional setup L_{ref} is such that the nondimensional domain size is $2\pi \times 2\pi\delta$ and U_{ref} is such that the nondimensional energy is on average unity. A fully-dealiased pseudo spectral spatial discretization, with a 128x128 physical grid, is used in conjunction with an adaptive fourth order Runge-Kutta time stepping scheme. The tendency of energy to cascade to larger scales obviates the need for increased resolution; this was verified using companion higher-resolution simulations. In order to observe regime transitions, the time evolution of higher order moments of vorticity need to be adequately represented, necessitating time steps that are $O(100)$ times smaller than required for stability.

In all simulations considered further, δ is fixed at 0.91. Simulations were considered for a number of values of α in the range $10^{-4} - 10^{-3}$. However, results are presented for the representative case of $\alpha = 2 \times 10^{-4}$. In particular each simulation for that value of α was also repeated with $\alpha = 4 \times 10^{-4}$ and the results were qualitatively unchanged.

0.4 Low-frequency variability and regime transitions

In the simulations considered, α variations in the range 10^{-4} to 10^{-3} lead to dissipation timescales of the order of 10^3 eddy turnover times, and an energy input rate due to forcing that is $O(10^3)$ times smaller than the nonlinear flux of energy in the system. In this sense, forcing and dissipation are both weak compared to nonlinearity in the dynamics of the model. Alternatively, the weakness of the linear damping results in a damping scale for energy that is larger than the size of the domain, allowing for energy to condense on to the largest scales (e.g., see Smith and Yakhot (1993)). Furthermore, in this regime, the model displays behavior that is somewhat analogous to a subcritical pitchfork bifurcation in the presence of noise (Bouchet and Simonnet (2009)). That is, under the influence of weak random forcing, the model switches randomly and abruptly between zonal and dipolar states, as

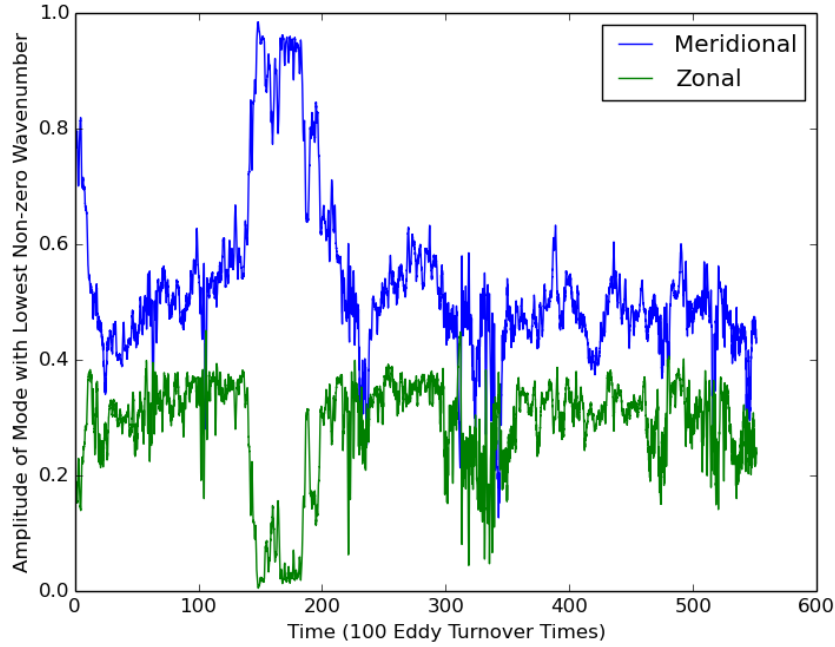


Figure 3: Amplitude of zonal and meridional modes with the lowest non-zero wavenumber indicate transition from a dipolar state to a zonal state and back.

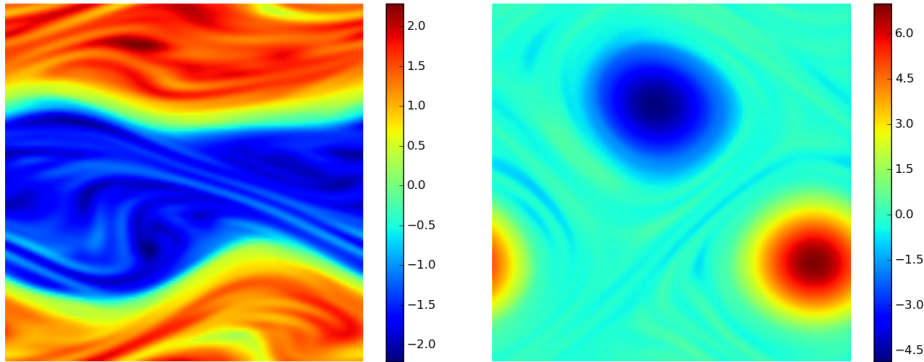


Figure 4: Vorticity field when the system is in a zonal state (left, time=15000) and when the system is in a dipolar state (right, time=26000) in the reference run.

shown in Figs. 3 and 4.

Amplitude of modes with the lowest non-zero wavenumber in zonal and meridional directions are plotted for a particular realization of the weak stochastic forcing in Fig. 3. We will use this run as the reference or truth run for further investigation of predictability. The transition from a dipolar state to a zonal state (around a time of 14000) and back (around a time of 20000) is evident in that figure. The snapshot of vorticity at a time of 15000 (left panel of Fig. 4) shows that the system has a larger zonal flow component as compared to the state of the system at time 26000 (right panel of Fig. 4). Consequently we will loosely refer to states of the system that are similar to that at time 15000 as “zonal” and states similar to that at time 26000 as “dipolar”. We also note that the kurtosis of the vorticity distribution is negative and small in the zonal state whereas it is positive and large in the dipolar state.

0.5 Ensemble Perturbations

Predictability is associated with the stability of the flow with respect to perturbations (errors) and their associated growth. For infinitesimal initial perturbations, error growth may be close to linear and the growing perturbations may be well described using a tangent linear approximation to the full nonlinear evolution equations. However, because of the possibility that the leading Lyapunov exponent is related to small scale instabilities in a multiscale system where predictability originates from the larger scales (Lorenz (1969); Boffetta et al. (2002)), the leading Lyapunov exponent is often of limited relevance to predictability. An associated common observation is that in predictability studies using infinitesimal perturbations, linear growth is seen over only an initial small fraction of the predictability time. Therefore, what is more relevant to predictability than the leading Lyapunov exponent is the evolution of finite size perturbations under the full nonlinear equations. Additionally, for a given norm, some perturbations with given spatial structures may rapidly amplify whereas others will grow more slowly and yet others decay.

Pazó et al. (2010) examined perturbation dynamics in extended chaotic systems via the generically named Lyapunov vectors. They demonstrated that one may, using the general method for the calculation of Lyapunov vectors, generate initial perturbation vectors that contain by construction different types of information about the chaotic trajectory dependent on the initial perturbation magnitude (infinitesimal or finite) and the evolution

interval for the calculation (finite or quasi-infinite; past, future or both).

Because of their ease of construction, knowledge of the past (flow dependency) and dynamical balance we have chosen to characterize spacetime chaos in the model using bred vectors (BV). BVs are finite perturbations generated (or bred) by evolving the perturbed system $\omega'(t) = \omega(t) + \delta\omega(t)$ where $\omega(t)$ the control trajectory under the full nonlinear governing equations. The perturbations themselves are rescaled to a given size ϵ periodically at a time interval T as follows. The difference between control and perturbed trajectories $\delta\omega(t + \delta t) = \omega'(t + \delta t) - \omega(t + \delta t)$ is computed at times $\delta t = nT$ for $n \in 1, \dots, N \in \mathbb{N}$ whereupon the perturbation is rescaled and the perturbed system redefined as $\omega'(t + \delta t) = \omega(t + \delta t) + \epsilon\delta\omega(t + \delta t)/\|\delta\omega(t + \delta t)\|$. The perturbation is now allowed to evolve freely until the next rescaling is scheduled at time $(n + 1)T$. The bred vector corresponds to the (finite) perturbation $\delta\omega(t)$ constructed at time t . We consider a range of values for the perturbation amplitude and rescaling time. In our setting that involves low frequency regime transitions, the rescaling time is smaller than the average transition time by between two and three orders of magnitude.

As control, we also consider backward Lyapunov vector perturbations and compute them in the standard fashion (Benettin et al., 1980). In this context, the amplitude of the perturbation is chosen to be 10^{-5} times the enstrophy norm of the fully equilibrated flow state to which perturbations are added and the full nonlinear governing equations are used. The amplitude rescaling time is chosen to be a characteristic eddy turnover time. As discussed further later, when longer rescaling time periods are chosen, the growth of perturbations leads to nonlinearities being significant. In such cases, the behavior of the perturbations is qualitatively similar to those of finite amplitude bred vector perturbations.

0.6 Predictability in Zonal and Dipolar Regimes

In order to examine the predictability of the model we first generate a truth trajectory which is simply a long run of the model over at least one regime transition (see Fig. 3). In order to mimic a simple data assimilation scheme, the large scales ($1 \leq k \leq 5$) of both control and perturbed trajectories are nudged every eddy turnover time to the true state, with the strength of nudging set so that the error of the control forecast was comparable on average to the standard deviation of the truth field at a lead time of about 30 eddy turnover times (see Fig. 5). Error is defined at the forecast time as the root mean square of the difference between the truth and control fields

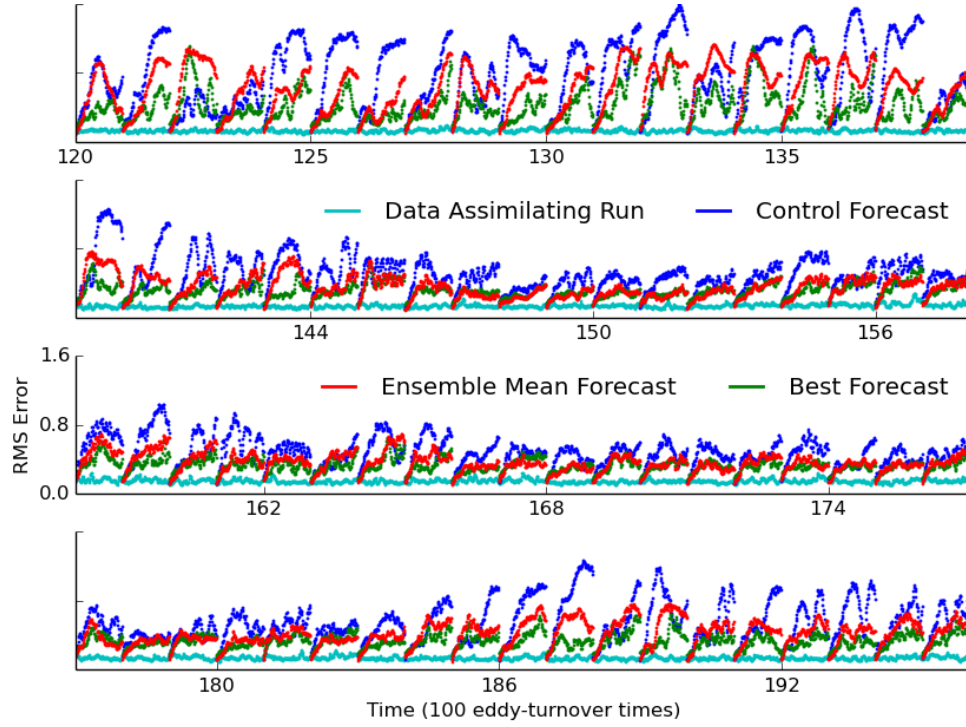


Figure 5: RMS error as a function of time between times 12000 and 20000. Error of the data assimilating run is shown in cyan, error of the control forecast in blue, error of the bred vector ensemble-mean in red and error of the best forecast member in green. When the system is in the zonal regime, as between times 15000 and 18000 approximately, error is seen to be smaller than when the system is in the dipolar regime.

and normalized by the root mean square of the truth field.

Stated in a different way, we are interested in predicting the true trajectory (at a certain lead time) in a situation where data-assimilation alone is incapable of achieving this. This is not because data-assimilation is ineffective: the strength and other characteristics of the periodic nudging that we use to mimic data-assimilation measures the effectiveness of data-assimilation. To mimic the limits of observing systems (large spatial scales and slow temporal scales are better observable while small spatial scales and fast temporal scales are not), we nudge only the large spatial scales and only at every eddy turnover time. On considering the smallness of errors in the data-assimilating run in Fig. 5 and the left panel of Fig. 6, we see that data-assimilation is effective. We will refer to the nudged control as the control analysis. A small forecast ensemble (control plus 14 perturbed members) is constructed about the control forecast using bred perturbation vectors (Toth and Kalnay (1997); O’Kane and Frederiksen (2008)). The bred vectors (BVs) were obtained using the method described above and initialized with random perturbation added to the control. Every rescaling period, the vector difference between the perturbed and control runs are rescaled to the initial amplitude using the RMS-norm and added to the control run.

Figure 5 shows RMS error as a function of time between times 12000 and 20000. In this plot, error of the data assimilating run is shown in cyan and is seen to be a small fraction (about 16%) of the natural variability. Error of the control forecast is shown in blue and is seen to be dependent on whether the flow is in a zonal or a dipolar state. In general, the forecast error is seen to be smaller when the system is in a zonal state (approximately between times 15000 and 18500). Error of the bred vector ensemble-mean is shown in red and is seen to be less than that of the control forecast. However, further analysis of the ensemble behavior is necessary to assess the utility of the ensemble prediction.

To partly address this, the error of the best forecast member is shown in green and it is seen that at least for some of the bred vector ensemble members, there are large reductions in forecast error. To further understand the improvement of forecast skill in individual members, we examined the spatial structure of the associated bred vector perturbations. On comparing the evolved bred vector and the error of the control forecast, we see a high degree of correlation between them, suggesting that the bred vector is effectively spanning the relevant low dimensional subspace of growing errors. This is the reason for the improved skill of certain of the ensemble members. It should be noted, however, that there are other members of the ensemble that end up spanning other subspaces than those related to errors

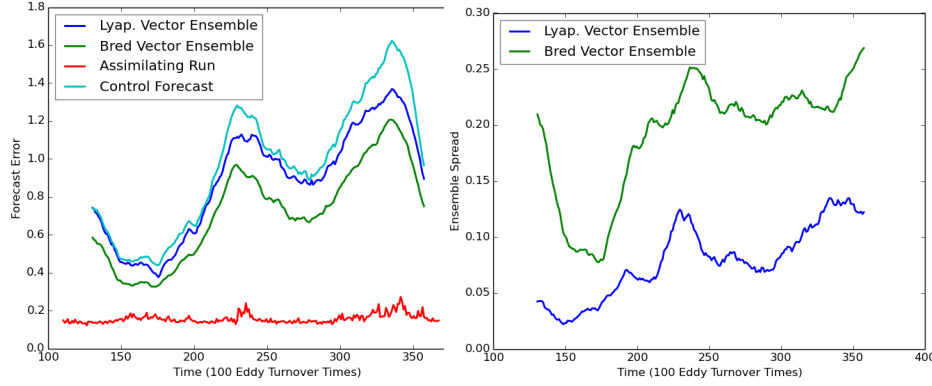


Figure 6: Forecast error (left) and ensemble spread (right) averaged over the forecast period as a function of time. Error of the data assimilating run is shown in red, error of the control forecast in cyan, error of the bred vector ensemble-mean in green and error of the Lyapunov vector ensemble-mean in blue. Also note that *analysis* error is shown for the assimilating run (even though the y -axis label is 'Forecast Error'). This is true in the other plots of 'error' as a function of time that follow.

in the control forecast. This reiterates the necessity of further analysis of the ensemble behavior to assess the utility of the ensemble prediction.

0.7 Ensemble behavior in terms of error and spread

It is traditional to consider the error-spread behavior of an ensemble prediction system to assess its utility. In addition to this, we find that in the present setting of a system that allows for multiple regimes, it is helpful to interpret the error-spread relationship by also examining individual plots of forecast error and spread as functions of time. This is presented in Fig. 6.

In the left panel of Fig. 6, it is seen that the forecast error is reduced, in both zonal and dipolar states, by a significant fraction in the bred vector ensemble whereas this reduction is smaller in the Lyapunov vector ensemble. The right panel of Fig. 6 shows spread as a function of time for the two ensembles. The larger spread of the BV ensemble suggests greater ensemble diversity than in the LV ensemble. Further, when the system is in the dipolar regime, the BV ensemble displays higher spread than when the system is in the zonal regime. The BV ensemble is thus telling us that there is a higher degree of uncertainty in predicting the state of the system when the system

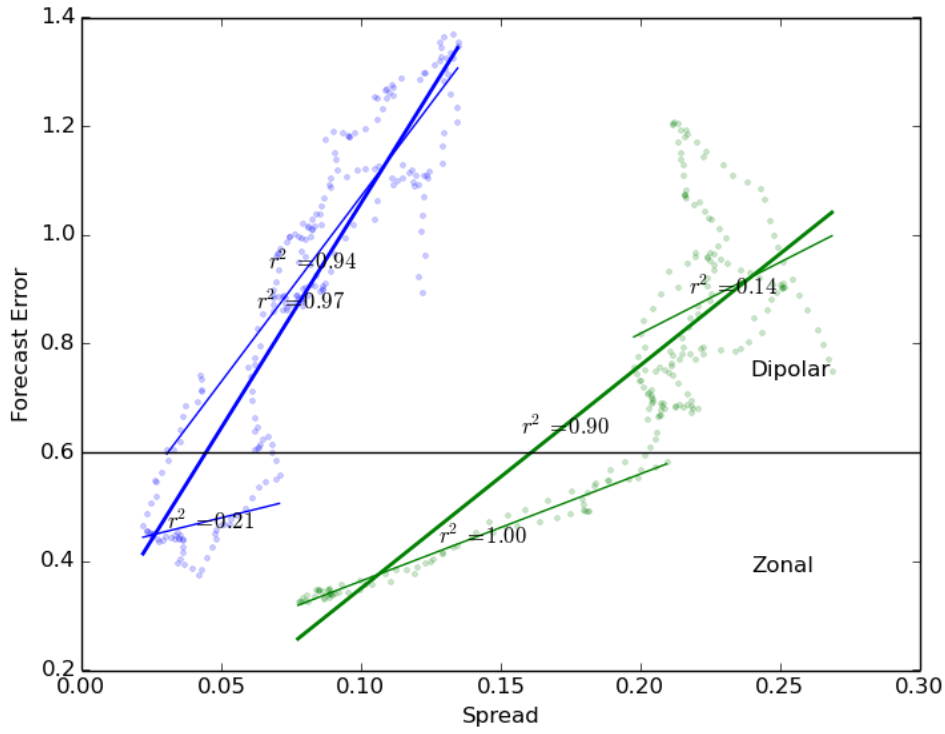


Figure 7: Scatter plot of forecast error against ensemble spread. Both quantities are averaged over the forecast period. LV ensemble is shown in blue and the BV ensemble in green

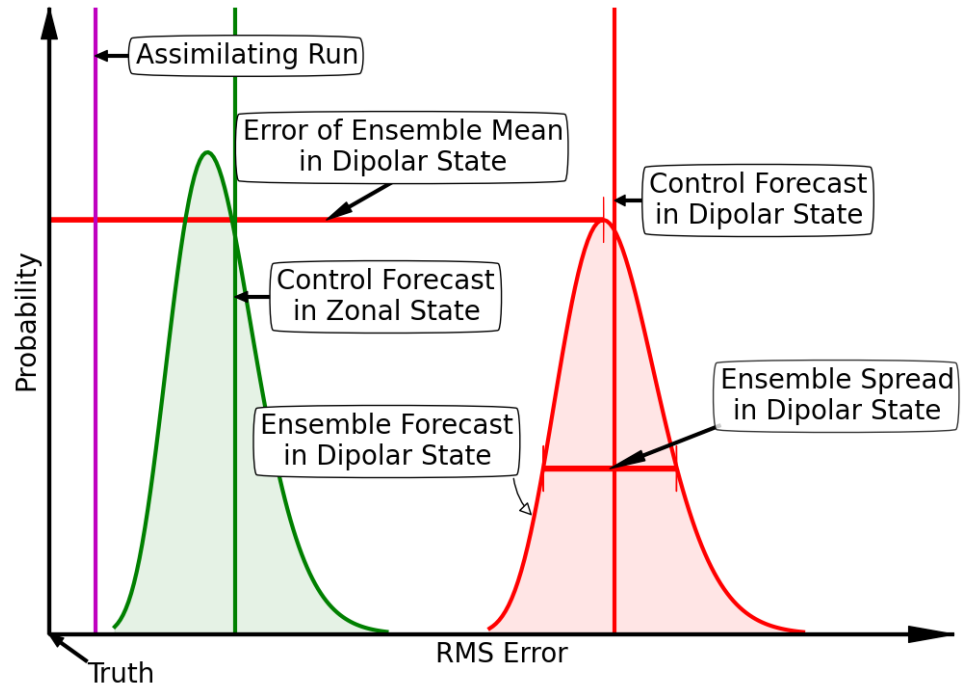


Figure 8: Schematic of the error-spread relationship realized in the Lyapunov vector ensemble. Reduction in error in both zonal and dipolar regimes is small. In the dipolar regime, even though the reduction in error is small and the error itself large, there is only a marginal increase in ensemble spread over that in the zonal regime.

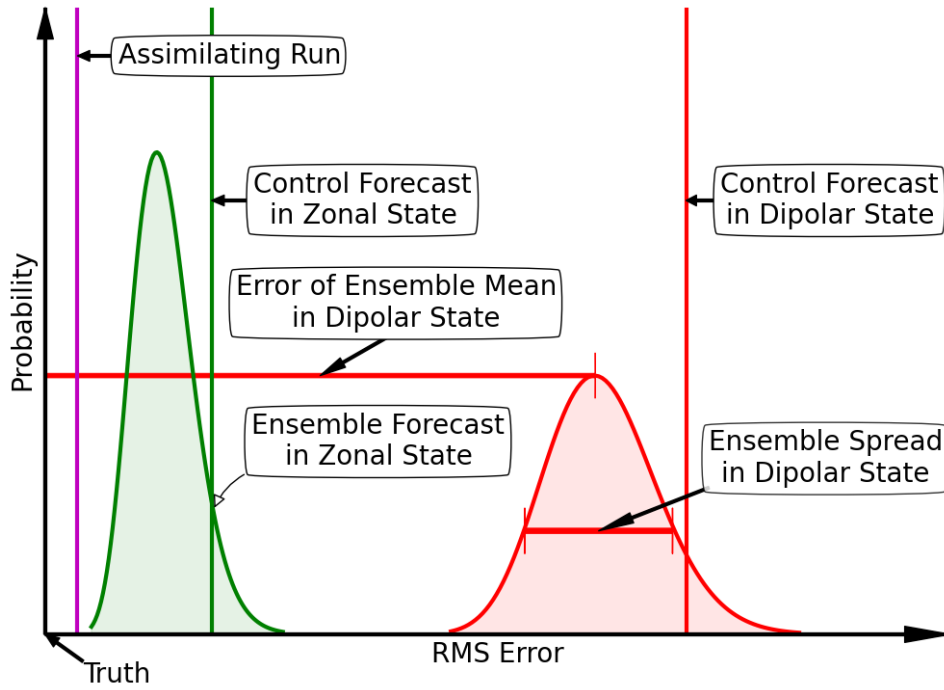


Figure 9: Schematic of the error-spread relationship realized in the Bred vector ensemble. A larger reduction in error, as compared to the LV ensemble, is seen in both regimes. The larger spread of the ensemble members in the dipolar regime as compared to the zonal regime identifies lower predictability in the dipolar regime.

is in the dipolar regime or likely that the predictability of the system when in the dipolar regime is poor. The LV ensemble corroborates this assessment of predictability in the two regimes.

Figure 7 shows a scatter plot of forecast error as a function of ensemble spread. Both quantities are averaged over the forecast period. LV ensemble is shown in blue and the BV ensemble in green. In this plot, the best-fit linear regression lines are also shown separately for the zonal and dipolar regimes and for the two regimes combined, and the r^2 values for the linear fits are indicated, where

$$r^2 = 1 - \frac{SS_{fit}}{SS_{tot}}.$$

Here SS_{fit} refers to the squared sum of the residuals with respect to the linear fit, SS_{tot} refers to the squared sum of the residuals with respect to the mean, and r^2 measures the “goodness” of the linear fit. r^2 is provided to avoid over-interpreting the fit: For example, in the zonal regime, while the linear fit is practically useless for the LV ensemble, it is meaningful for the BV ensemble. Finally, even when r^2 values are reasonably large, systematic deviations of the scatter plot from the linear fit is a further measure of inappropriateness of the linear fit for the data.

The increased error and spread in the dipolar regime as compared to the zonal regime for the BV ensemble reiterates the reduced predictability of the dipolar regime as compared to the zonal regime. While the differing relationship between error and spread in the dipolar and zonal regimes is seen in the LV ensemble as well, this difference is more muted. That is, the increased error in the dipolar region is accompanied by only a modest increase in spread. This suggests the possibility that the LV ensemble is less efficient as compared to the BV ensemble. Indeed, the behavior of the LV and BV ensembles may be described schematically with Figs. 8 and 9. In the LV ensemble (Fig. 8) reduction in error in both zonal and dipolar regimes is small. In the dipolar regime, even though the reduction in error is small and the error itself is large, the ensemble spread increases only marginally over that in the zonal regime. However, in the BV ensemble (Fig. 9) reduction in error in both zonal and dipolar regimes is larger than in the LV ensemble. Further, in the dipolar regime, the larger spread of the ensemble in the dipolar regime as compared to the zonal regime emphasizes lower predictability in the dipolar regime. That is, the different predictability characteristics of the zonal and dipolar regimes are borne out better by the differing error-spread relationships in the two regimes by the BV ensemble.

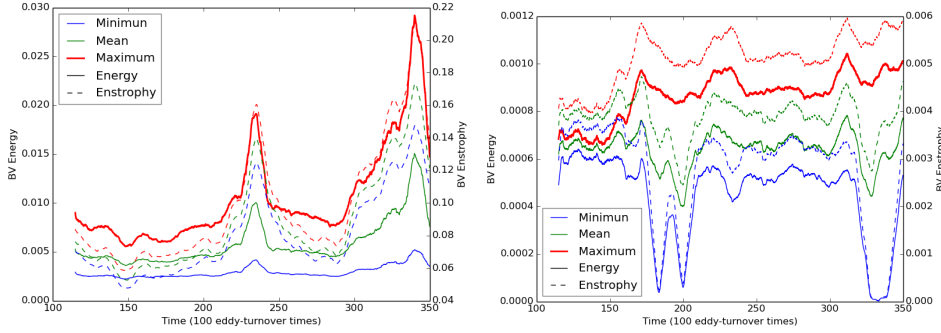


Figure 10: Minimum (blue), mean (green), and maximum (red) energy (solid) and enstrophy (dashed) over the ensemble of BV (left) and LV (right) perturbations. Maximum BV energy is seen to correlate best with forecast error.

0.8 Flow stability and sensitivity of BVs to rescaling amplitude and period

As discussed previously, predictability is associated with the stability of the flow with respect to perturbations (errors) and their associated growth. Figure 10 shows the energy and enstrophy of the BV perturbations in the left panel and those of the LV perturbations in the right panel. First, forecast error in Fig. 6 is seen to correlate better with the maximum of the BV energy and enstrophy than with those of the LV perturbations. Indeed, we suspect that this correlation is causal. That is, increased forecast error when the system is in the dipolar regime is likely due to increased instability of flow in that regime. Further, the dominant similarity of energy and enstrophy norms of the LV perturbations suggests that the LV perturbations are largely concentrated at a single scale. In contrast, a variable relationship between enstrophy and energy norms of the BV perturbations suggests that these perturbations are expressed on a wider range of scales that change dynamically.

While the expression of BVs is typically enhanced in localized regions of large shear, it is difficult to develop an intuitive understanding of the structure of BVs for the following reason: On examination of various pairs of BVs, we find that not only do visually different bred vectors lead to significantly different forecasts (not surprising,) but that visually identical-looking bred vectors lead to significantly different forecasts. For this reason, we consider some integrated aspects of the BVs to further analyze them. Previously,

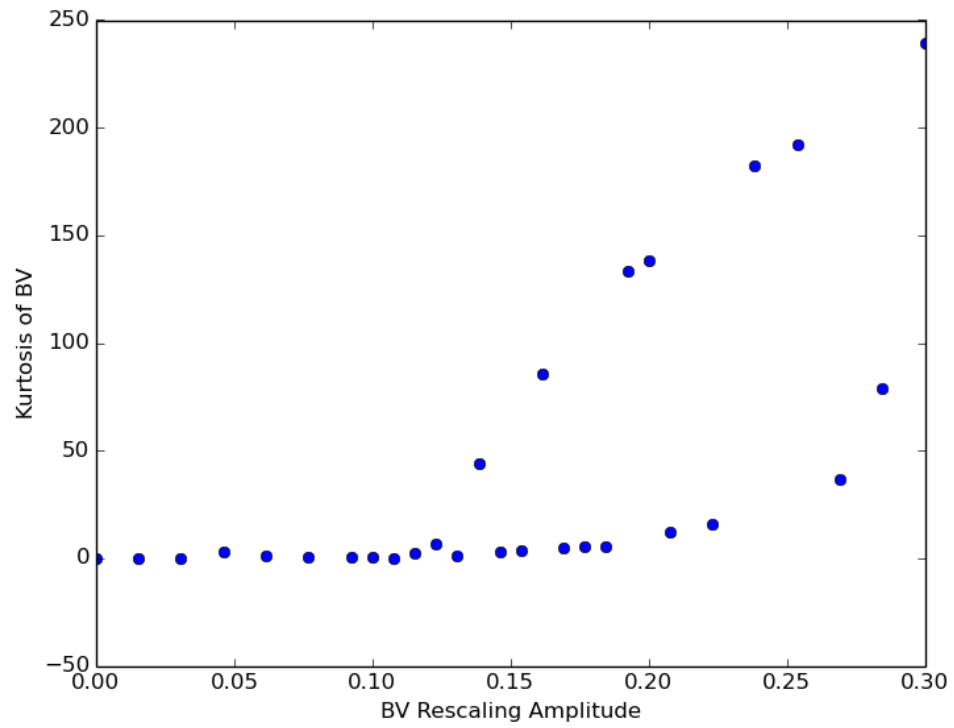


Figure 11: Kurtosis of BV perturbation as a function of rescaling amplitude. A pitchfork bifurcation is seen to occur when the rescaling amplitude is about 0.12.

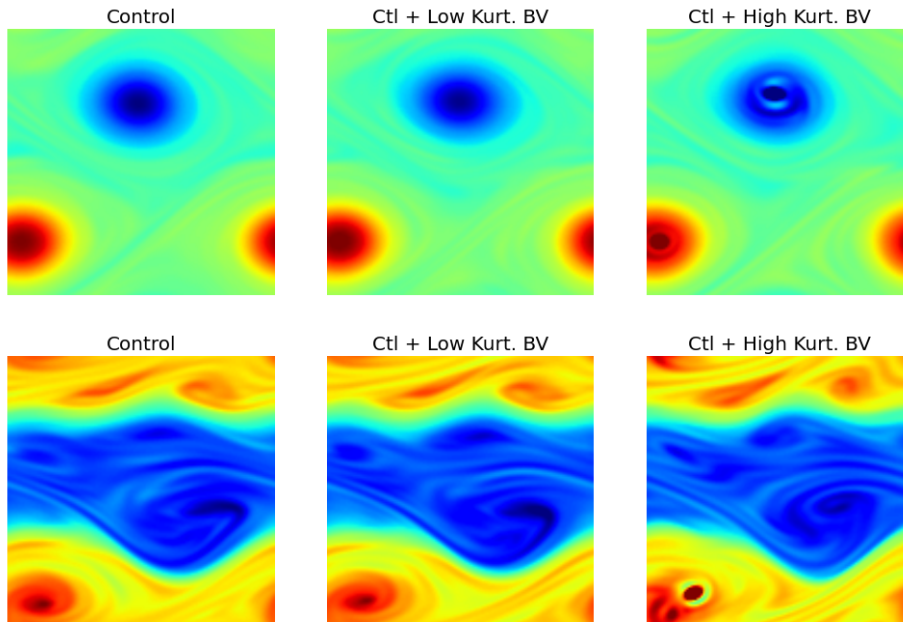


Figure 12: Low and high kurtosis bred vectors in the dipolar state (top) and zonal state (bottom)

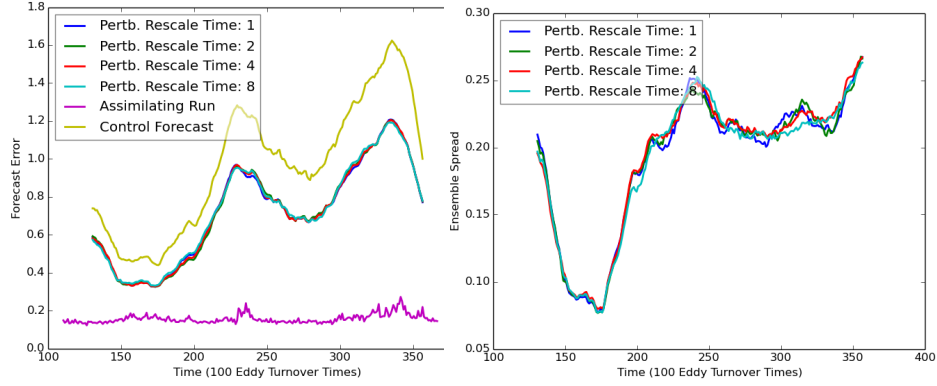


Figure 13: Forecast error (left) and ensemble spread (right) averaged over the forecast period as a function of time. In this series of four experiments, the amplitude of the perturbation vectors are rescaled at 1, 2, 4, and 8 eddy turnover times and the amplitude to which the perturbations are rescaled is large (0.2 times the initial base enstrophy). In this case of finite amplitude bred vector perturbations, the dependence of forecast error and ensemble spread on rescaling time is seen to be very weak.

we have considered energy and enstrophy norms of the BV and LV perturbations. Presently, we consider kurtosis of the perturbations. Kurtosis is defined in the usual fashion as the deviation from a Gaussian distribution of the fourth moment of the spatial distribution of vorticity perturbation. Figure 11 shows the kurtosis of the bred vector perturbations for a range of rescaling amplitudes, and a pitchfork bifurcation is seen to occur when the perturbation amplitude is about 0.12. At this bifurcation, a branch with high kurtosis comes into existence. Further analysis of this branch suggests that it corresponds to a family of instability that involves a localized distortion of the most cyclonic or anticyclonic regions of the flow. Control vorticity fields and the sum of control field and representative low and high kurtosis bred vectors when the system is in the dipolar regime (top row) and zonal regime (bottom row) are shown in Fig. 12.

0.8.1 Dependence of error and spread on perturbation rescaling period

In Fig. 11, we saw how different kinds of instabilities are captured depending on the rescaling amplitude of the BVs. Likewise, it is possible that different growing modes of the system are captured depending on the rescaling period

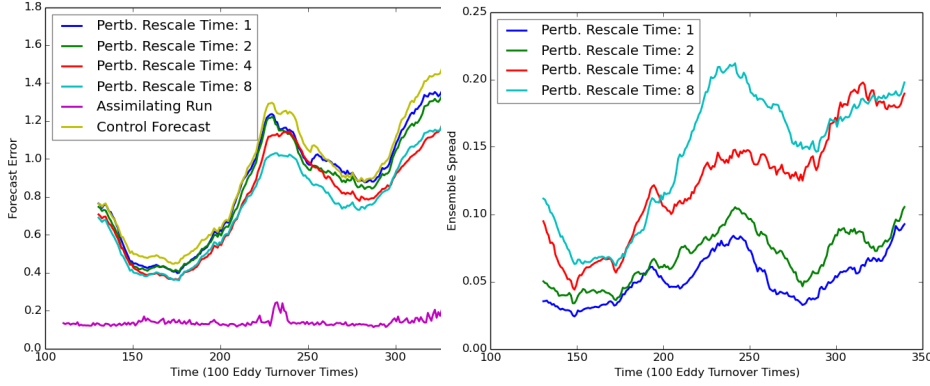


Figure 14: This series of four experiments are similar to those in fig. 13: The only difference is that the amplitude to which the perturbations are rescaled is small (10^{-5} times the initial base enstrophy). In this case, the dependence on rescaling time is strong: The decreased error and increased spread in the two cases where the rescaling times are 4 and 8 eddy turnover times is likely due to the perturbations having grown large and a manifestation of the nonlinear filtering effect of finite-amplitude evolved perturbations.

for the BVs. In a shear-dominated flow as we presently consider, this could be for example due to reasons of non-normality of the linear operator. Or such dependence could be expected because of nonlinear saturation kinds of effects. For this reason, a series of experiments were conducted wherein the rescaling period was varied between 1 and 8 large-scale eddy turnover times. Figure. 13 shows the forecast error (left) and ensemble spread (right) averaged over the forecast period as a function of time for the case where the rescaling amplitude is large. In this series of four experiments, the amplitude of the perturbation vectors are rescaled at 1, 2, 4, and 8 eddy turnover times and the amplitude to which the perturbations are rescaled is large (0.2 times the initial base enstrophy). In this case of finite amplitude bred vector perturbations, the dependence of forecast error and ensemble spread on rescaling time is seen to be very weak. On the other hand, when the same experiments were repeated for the case when the rescaling amplitude is smaller, (10^{-5} times the initial base enstrophy), a stronger dependence of error and spread on rescaling time is seen (Fig. 14). The decreased error and increased spread in the two cases where the rescaling times are 4 and 8 eddy turnover times is likely due to the perturbations having grown large and a manifestation of the nonlinear filtering effect of finite-amplitude evolved

perturbations.

0.8.2 Error and spread of random rescaling BV perturbations

We finally consider an ensemble of BV perturbations in which the rescaling amplitude and rescaling period are both chosen randomly; rescaling amplitude was chosen based on an enstrophy norm from a uniform distribution between 10^{-5} and 0.2 times the initial base enstrophy and rescaling period was chosen randomly from a uniform distribution between 1 and 8 eddy turnover times. It is seen in Fig. 15 that the behavior of this ensemble is not significantly different from a BV ensemble in which the rescaling amplitude and rescaling period are both held constant (rescaling amplitude of 0.2 times base enstrophy and a rescaling period of 8 turnover times). Thus given the robustness of error and spread behavior for finite amplitude perturbations, it seems that guesswork may be largely removed from the use of BVs by choosing such a random rescaling strategy, as long as the range of rescaling parameter values are chosen reasonably. However, this finding needs to be verified before being used in other systems.

0.9 The role of small scales

It was anticipated that the higher order non-Gaussian nature of the distribution of vorticity that at least some of the larger amplitude bred vectors exhibited may be of importance in identifying small scale coherent error structures and therefore play a dynamical role in predictions. In order to examine this possibility, we conducted experiments in which nudging was also considered at small scales. That is, whereas in the default setting, assimilation was performed only at the large scales, a second setting was also considered wherein assimilation was performed at all scales. The hypothesis here being that when assimilation is performed at small scales, the coherence of dynamically important structures (that possess small scale features) in the BV perturbations is broken, thus reducing the effectiveness of BV perturbations in representing such structures.

Figure. 16 shows the forecast error (left) and ensemble spread (right) when assimilation is performed at all the scales in the system (green), rather than at only the large scales of the system (blue). Firstly, among the two assimilating runs, it is seen that when assimilation is also performed at small scales, analysis error is reduced (in comparison to the default case wherein assimilation is only performed at large scales). However, error in the two

control forecasts initialized with the two differently assimilating (large scale only versus all scale) is far more similar. This suggests ineffectiveness of performing assimilations at smaller scales. (Such ineffectiveness is likely related to the dynamics of backscatter—or how the small scales affect the large scales; e.g., see Nadiga (2008)). That is, even though error at small scales is held down by data assimilation at those scales, the incremental reduction in analysis error over the (default) assimilation setup wherein assimilations are only performed at large scales, does not translate into improved predictions.

In the ensemble forecast context, it actually so happens that performing data assimilation at the smaller scales has a *deleterious* effect. This can be seen in the slight increase in ensemble mean forecast error at most times when assimilation is also performed at small scales. Finally, the increased ensemble-mean forecast error is accompanied by reduced ensemble spread. This suggests that in the case when smaller scales are assimilated, the diversity of the BVs is actually reduced. Such combined behavior of error and spread highlights the importance of considering the role of instabilities at small scales in flow predictions. When restoring is present at the small scales, instabilities at these scales or the coherent development of structures that include these scales are inhibited in BVs. This either precludes or partially thwarts the ability of BVs to highlight incipient dynamically important regions and evolve the associated structures to compensate co-located control forecast errors.

0.10 Discussion and conclusion

We considered a model based on the barotropic vorticity equation and in which both dissipation and stochastic forcing are weak compared to non-linearity. (Note that weakly dissipative regimes are generally inaccessible to state of the art general circulation models because of resolution requirements.) This system exhibits the phenomenon of low-frequency regime transitions. A dynamical explanation of low-frequency regime transitions in a system is as follows: if the system supports multiple equilibria, then noise can induce transitions between such equilibria through a form of stochastic resonance. Zonal flows and dipoles are well recognized as statistical mechanical equilibria of the system we consider. Then, specifically, at any given time, the system is in a basin of attraction of a particular attractor (regime). Cumulative effect of stochastic forcing, however, pushes the system over the attractor boundary so that the system finds itself in the basin

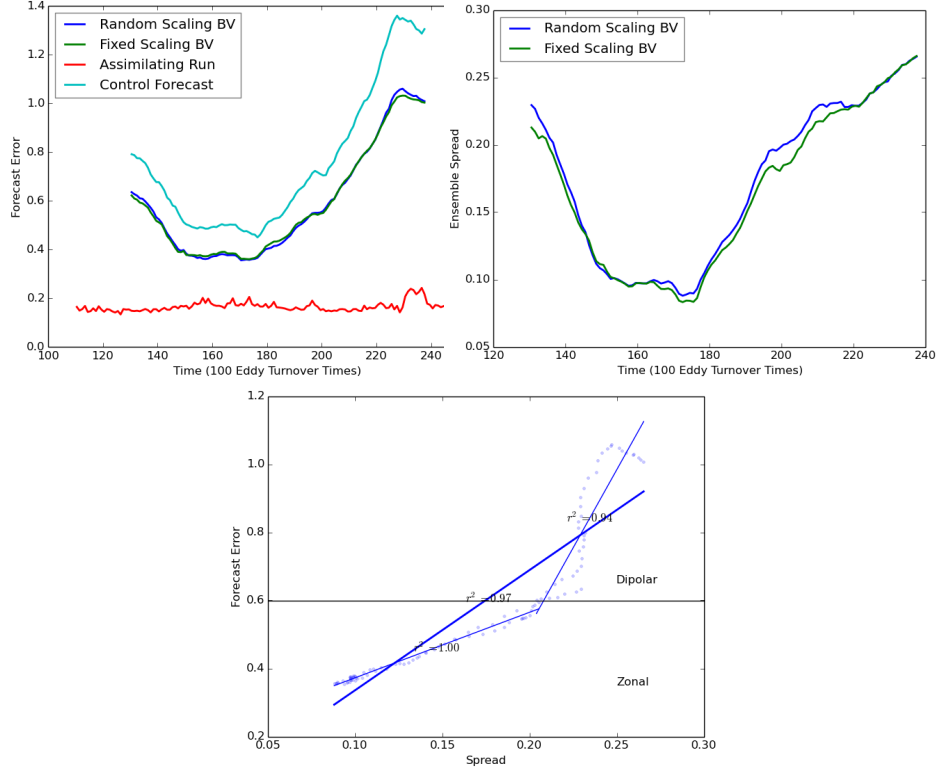


Figure 15: Random rescaling versus fixed rescaling BV ensembles. When both rescaling amplitude and rescaling period are drawn from uniform distributions (see text for ranges), the ensemble behavior is similar to that of an ensemble with fixed (finite) rescaling amplitude and fixed (long) rescaling period.

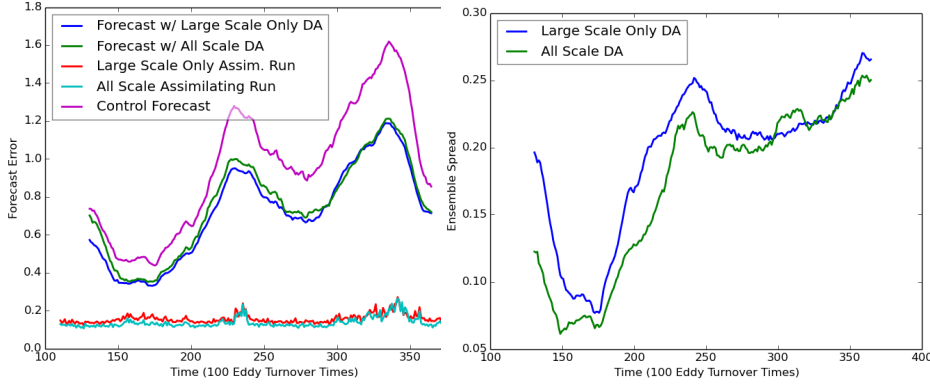


Figure 16: When data assimilation is applied at all scales (green), it is seen that the forecast error increases slightly whereas the ensemble spread mostly decreases as compared to when data assimilation is applied only to the large scales (blue). This points to the dynamical importance of small scales to improving predictions.

of attraction of a different attractor (different regime). Dynamical processes then lead to a relaxation of the system onto the different attractor (regime) and the process continues.

We were interested in the predictability of flow in the different regimes and in the role small scales play in such predictions. We were also interested in the role small scales play in low-frequency regime transitions. To this end, we conducted prediction experiments that use a simple data-assimilation scheme. Indeed the process of data assimilation is emulated by nudging the large scales of the system to truth on the large eddy turnover timescale. While the estimate of the state of the system using such a scheme was good, predictions based on that estimate alone (control forecast) were deficient. We then examined the use of bred vector perturbations and Lyapunov vector perturbations in improving the control forecast. We find that ensembles that use finite amplitude BV perturbations are more effective at reducing forecast error and are more reliable as compared to ensembles that use LV perturbations. This is consistent with previous understanding and explanations of predictability in multiscale systems that emphasize the importance of the growth of finite amplitude perturbations as opposed to purely linear instabilities. Indeed, the advantages of BV perturbations that we demonstrate in this article are automatically realized when data assimilation is based on a genuine dynamically evolving ensemble (e.g., see Nadiga et al.,

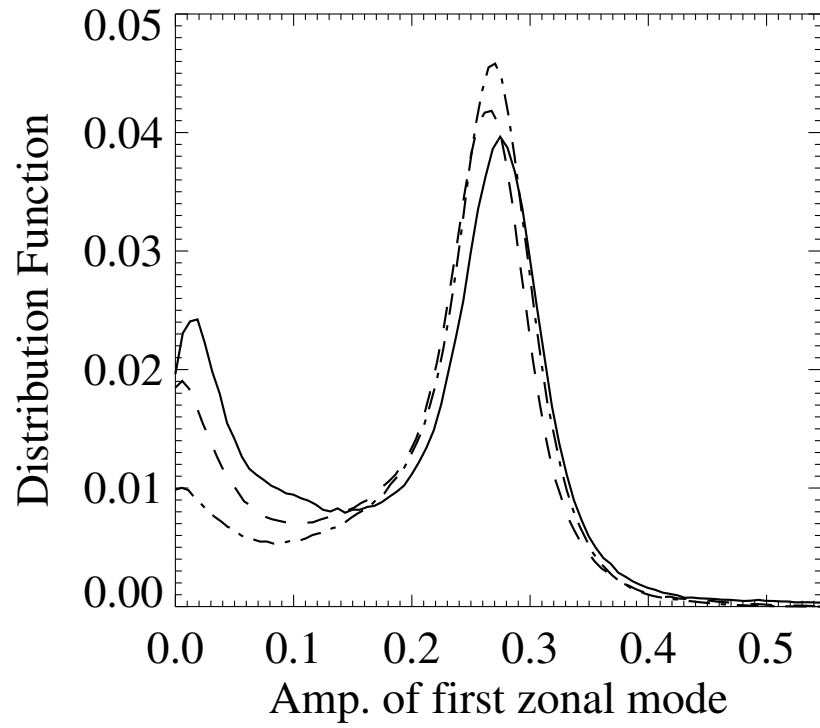


Figure 17: Distribution function of amplitude of energy in the first zonal mode. When the proportion of forcing at small scales is increased progressively from solid to dashed to dot-dashed, the dipolar state is increasingly preferred and transitions between the zonal and dipolar states become less frequent.

2013, and references therein).

Focusing further attention on finite amplitude BV perturbations, we found that forecast errors were smaller than that of the control forecast for some of the members. For such members, the error reduction was seen to be achieved by a process wherein dynamically important unstable subspaces identified by BV perturbations evolve into structures that compensate regions of control forecast error.

Next, we found that the system has lesser predictability when it is in the dipolar regime as compared to the zonal regime. Indeed the peaks of vorticity that are characteristic of the dipolar regime make the flow in that regime more unstable and constitutes the primary reason for lesser predictability of the system when in that regime. This instability is however unlikely to be the usual asymptotic linear instability alone. Our experiments suggest that instability of finite amplitude perturbations play an equally important role. In ensemble prediction experiments that use finite amplitude BV perturbations and those that use LV perturbations, forecast errors of ensemble predictions are seen to correlate far better with measures of instability as provided by the finite amplitude BV perturbations. Indeed, by systematically varying the amplitude of the perturbations, evidence for a new branch of instability at a finite amplitude was presented. Nevertheless, the horizon of predictability in either of the regimes was short compared to characteristic time scales associated with processes that lead to regime transitions, thus precluding the possibility of predicting such transitions.

The ensemble predictions were also analyzed for their utility by examining forecast error and ensemble spread and their relationship in the two regimes. The error-spread relationship was seen to be different in the two regimes with a much stronger linear relationship with a positive correlation being realized when the system was in the zonal regime. The most uncertain aspect of prediction when the system is in the dipolar state is the position of peak cyclonic and anti-cyclonic vorticities and the ensemble-mean averages over this uncertainty. Consequently, while there was a reduction in error of the ensemble-mean over that of the control forecast, it was, in a sense, not very useful or skillful. This explains the weaker relationship between error and spread in the dipolar regime. Further, smaller error and better error-spread relationship was realized with the finite amplitude BV ensemble than with the LV ensemble.

A further series of experiments demonstrated that as long as the amplitude of the perturbations were large enough (say to capture the new branch of instability that was identified), the behavior of the ensemble was robust to rescaling period and amplitude. Indeed the ensemble behavior with a

random rescaling strategy was statistically no different from that with a fixed rescaling strategy. Next, that the small scales play a significant role in predictions was established by conducting experiments in which the small scales were either included or not included in the simple data assimilation procedure. In experiments that nudged the small scales as well, the ability of BV perturbations to carry information about dynamically important structures was likely compromised leading to larger forecast errors and smaller ensemble spread. This led us to form a hypothesis about the role of small scales in initiating low-frequency regime transitions: If the small scales play a role in initiating low-frequency transitions, then extending stochastic forcing to the smaller scales should suppress transitions. Figure 17 shows that in experiments where forcing was confined to small scales or where a larger proportion of the forcing was at small scales, no transitions were observed. In experiments where transitions were observed, the transitions became infrequent as the proportion of forcing at small scales (still small) increased. These experiments therefore verify the importance of small scales and the process of backscatter in initiating low-frequency regime transitions in the model.

The relevance of this study to the ocean-atmosphere system is twofold: a) It is well recognized that the timescales for low frequency variability in the climate system are largely set by the ocean with the atmospheric state acting as a source of stochasticity. However, the atmospheric forcing can be correlated at large spatial scales (atmospheric teleconnections). The role of such stochastic forcing in determining the ocean state is only beginning to be considered (e.g., see OKane et al., 2013). This study may be seen as preliminary work towards such a characterization. Thus if (as is likely) ocean circulation is predisposed to supporting multiple equilibria, then weak stochastic forcing by the atmosphere has the potential to induce transitions in the ocean state by a form of stochastic forcing. b) We find that coherent evolution of small scale structures likely plays a role in initiating low-frequency transitions between states with very different large scale structure and that accounting for the presence of such dynamically important small scale structures is important for predictions. An implication of this finding for models that do not explicitly resolve such small scales, but rather parametrize them in a generic fashion (e.g., see Frederiksen and O’Kane, 2008, and references therein), is a likely reduction in its predictive capability.

0.11 acknowledgments

TJO is supported by an Australian Research Council Research Fellowship.

Bibliography

- Benettin, Giancarlo, Galgani, Luigi, Giorgilli, Antonio, and Strelcyn, Jean-Marie. 1980. Lyapunov characteristic exponents for smooth dynamical systems and for Hamiltonian systems; a method for computing all of them. Part 1: Theory. *Meccanica*, **15**(1), 9–20.
- Benzi, Roberto, Parisi, Giorgio, Sutera, Alfonso, and Vulpiani, Angelo. 1982. Stochastic resonance in climatic change. *Tellus*, **34**(1), 10–16.
- Boffetta, Guido, Cencini, Massimo, Falcioni, Massimo, and Vulpiani, Angelo. 2002. Predictability: a way to characterize complexity. *Physics reports*, **356**(6), 367–474.
- Bouchet, Freddy, and Simonnet, Eric. 2009. Random changes of flow topology in two-dimensional and geophysical turbulence. *Physical review letters*, **102**(9), 094504.
- Charney, Jule G, and DeVore, John G. 1979. Multiple flow equilibria in the atmosphere and blocking. *Journal of the Atmospheric Sciences*, **36**(7), 1205–1216.
- Chavanis, PH, and Sommeria, J. 1996. Classification of self-organized vortices in two-dimensional turbulence: the case of a bounded domain. *Journal of Fluid Mechanics*, **314**, 267–297.
- Dansgaard, Willi, White, JWC, and Johnsen, SJ. 1989. The abrupt termination of the Younger Dryas climate event. *Nature*.
- Frederiksen, Jorgen S, and O’Kane, Terence J. 2008. Entropy, closures and subgrid modeling. *Entropy*, **10**(4), 635–683.
- Lorenz, Edward N. 1969. The predictability of a flow which possesses many scales of motion. *Tellus*, **21**(3), 289–307.

- Loxley, PN, and Nadiga, BT. 2013. Bistability and hysteresis of maximum-entropy states in decaying two-dimensional turbulence. *Physics of Fluids (1994-present)*, **25**(1), 015113.
- Nadiga, Balasubramanya T, Casper, W Riley, and Jones, Philip W. 2013. Ensemble-based global ocean data assimilation. *Ocean Modelling*, **72**, 210–230.
- Nadiga, BT. 2008. Orientation of eddy fluxes in geostrophic turbulence. *Philosophical Transactions of the Royal Society A: Mathematical, Physical and Engineering Sciences*, **366**(1875), 2489–2508.
- Nakamura, Hisashi, Nakamura, Mototaka, and Anderson, Jeffrey L. 1997. The role of high-and low-frequency dynamics in blocking formation. *Monthly weather review*, **125**(9), 2074–2093.
- O’Kane, Terence J, and Frederiksen, Jorgen S. 2008. A comparison of statistical dynamical and ensemble prediction methods during blocking. *Journal of the atmospheric sciences*, **65**(2), 426–447.
- OKane, Terence J, Matear, Richard J, Chamberlain, Matthew A, Risbey, James S, Sloyan, Bernadette M, and Horenko, Illia. 2013. Decadal variability in an OGCM Southern Ocean: Intrinsic modes, forced modes and metastable states. *Ocean Modelling*, **69**, 1–21.
- Pazó, Diego, Rodríguez, Miguel A, and López, Juan M. 2010. Spatio-temporal evolution of perturbations in ensembles initialized by bred, Lyapunov and singular vectors. *Tellus A*, **62**(1), 10–23.
- Qiu, Bo, and Miao, Weifeng. 2000. Kuroshio path variations south of Japan: Bimodality as a self-sustained internal oscillation. *Journal of Physical Oceanography*, **30**(8), 2124–2137.
- Smith, Leslie M, and Yakhot, Victor. 1993. Bose condensation and small-scale structure generation in a random force driven 2D turbulence. *Physical review letters*, **71**(3), 352.
- Toth, Zoltan, and Kalnay, Eugenia. 1997. Ensemble forecasting at NCEP and the breeding method. *Monthly Weather Review*, **125**(12), 3297–3319.
- Williams, Paul David, Read, PL, and Haine, TWN. 2003. Spontaneous generation and impact of inertia-gravity waves in a stratified, two-layer shear flow. *Geophysical research letters*, **30**(24).